DOI: 10.1002/ejic.200500875

In situ HT-XRD Study on the Formation of Hexagonal Ammonium Tungsten Bronze by Partial Reduction of Ammonium Paratungstate Tetrahydrate

Imre Miklós Szilágyi,*[a] Ferenc Hange,[b] János Madarász,[a] and György Pokol[a]

Keywords: Tungsten / Reduction / In situ studies / X-ray diffraction / X-ray photoelectron spectroscopy / Solid-state ^{1}H NMR spectroscopy

Hexagonal ammonium tungsten bronze, $(NH_4)_{0.33-x}WO_{3-y}$, is a possible constituent of the intermediate "tungsten blue oxide" in non-sag (NS) tungsten production and a material of chromogenic and sensor interest. Its formation has been studied by in situ high-temperature powder X-ray diffraction (HT-XRD) accompanied by semiquantitative phase analysis through the partial thermal reduction of ammonium paratungstate tetrahydrate, $(NH_4)_{10}[H_2W_{12}O_{42}]\cdot 4H_2O$, in flowing 10 % H_2/He. The effect of the heating program on the formation of the title compound has been discussed. Highly crystalline, monophasic hexagonal ammonium tungsten bronze prepared by partial reduction of ammonium paratungstate tetrahydrate has been characterised by high-precision powder XRD, X-ray photoelectron spectroscopy (XPS), chemical analysis and solid-state ^{1}H NMR spectroscopy (^{1}H-MAS-NMR).

Introduction

Hexagonal ammonium tungsten bronze (HATB), $(NH_4)_{0.33-x}WO_{3-y}$, is one of the compounds that may be intermediates in the powder metallurgical production of tungsten lamp filaments. Partial reduction of the starting material, ammonium paratungstate tetrahydrate (APT), $(NH_4)_{10}[H_2W_{12}O_{42}]\cdot 4H_2O$, between 400 and 600 °C produces an intermediate product (called "tungsten blue oxide"), which is a possible mixture of different phases. It is doped with K, Al and Si that ensure, after complete reduction in hydrogen, an overlapping crystallite structure of tungsten powder, which finally provides appropriate mechanical stability (a so-called "non-sag" feature) to tungsten filaments even at high operating temperatures in lamps.[1–3] Among the possible constituents of "tungsten blue oxide" (an X-ray amorphous phase, WO_3, $WO_{2.9}$, $WO_{2.72}$, WO_2 and tungsten bronzes[1,2,4–7]), hexagonal ammonium tungsten bronze may have an important role in the doping process because of its ion-exchange property.[4,5,8,9]

Furthermore, for applications in electrochromic devices,[1,10–14] humidity[15,16] and gas sensors[17–21] as well as secondary batteries,[22] metastable tungsten oxides and oxide bronzes have attracted much attention in the past decades due to their open-tunnel structures.[1,2,23,24] Hexagonal ammonium tungsten bronze is an interesting member of these compounds because of its mixed proton and electron conductivity[25] and, in addition, hexagonal WO_3 can be produced by its oxidation,[26] the latter being one of the most studied tungsten oxides.[22,27–29] Besides hydrothermal[25,30] and solvothermal[31,32] synthetic methods, the partial reduction of APT is also a viable way of preparing the hexagonal ammonium tungsten bronze for these fields of interest.

For further studies on the various aforementioned reactions and applications of the title compound, it is advisable to obtain a deeper insight into its formation through the partial reduction of APT. In previous studies, when heating APT at a rate of 5–10 °C min^{-1}, hexagonal ammonium tungsten bronze readily appeared between 350 and 600 °C but was accompanied by some other phases (monoclinic, orthorhombic or hexagonal WO_3 in air,[1,2,33–37] tetragonal hydrogen tungsten bronze, $WO_{2.9}$, $WO_{2.72}$ and WO_2 in reducing gases[1,2,7,37–40] and X-ray amorphous phase in all cases). On the other hand, a monophasic, crystalline and/or partly amorphous hexagonal ammonium tungsten bronze could be produced when APT was decomposed in a furnace between 300 and 500 °C in reducing[41–45] or inert gases.[46]

In an attempt to explain the effect of the heating conditions on the partial reduction of APT, we report here our results obtained by in situ high-temperature powder X-ray diffraction (HT-XRD) in flowing 10 % H_2/He on the formation and thermal stability of hexagonal ammonium tungsten bronze. Supported by the results of our HT-XRD measurements and also by earlier studies,[1,2,7,37–46] we have proposed a model for the formation of the title compound through the partial reduction of APT. In harmony with this model, HATB has been prepared in a monophasic, highly

[a] Institute of General and Analytical Chemistry, Budapest University of Technology and Economics,
Szt. Gellért tér 4, 1111 Budapest, Hungary
Fax: +36-1-463-3408
E-mail: imre.szilagyi@mail.bme.hu
[b] GE Hungary ZRt., GE Consumer & Industrial Lighting,
Váci út 77, 1340 Budapest, Hungary

crystalline form and its composition and structure have been studied by high-precision powder XRD, X-ray photoelectron spectroscopy (XPS), chemical analysis and solid-state ^{1}H NMR spectroscopy (^{1}H-MAS-NMR).

Results and Discussion

Formation and Thermal Stability of Hexagonal Ammonium Tungsten Bronze

On the basis of earlier studies,[43–45] an annealing temperature of 400 °C seemed to be the most suitable for the formation of the monophasic title compound when heating APT in a furnace in a reducing gas. This process (fast heating of APT followed by an isothermal period) has been modelled by in situ HT-XRD measurements in flowing 10% H_2/He.

Straight after (1 min) rapid heating (100 °C min^{-1}) of APT to 400 °C, hexagonal ammonium tungsten bronze, HATB (ICDD 42-0452), tetragonal hydrogen tungsten bronze, THTB, H_xWO_{3-y} (ICDD 23-1448), and an X-ray amorphous phase were identified in the XRD pattern (Figure 1). The 2θ = 23.702° reflection of HATB (I/I_0 = 65%) and the 2θ = 22.980° reflection of THTB (I/I_0 = 50%) were used for semiquantitative phase analysis. The amounts of crystalline hexagonal bronze and tetragonal bronze were 69% and 31%, respectively (Figure 2). This is much higher than in the case of heating APT slowly (5 °C min^{-1}) to 450 °C, whereby the proportion of HATB was 34%.[47]

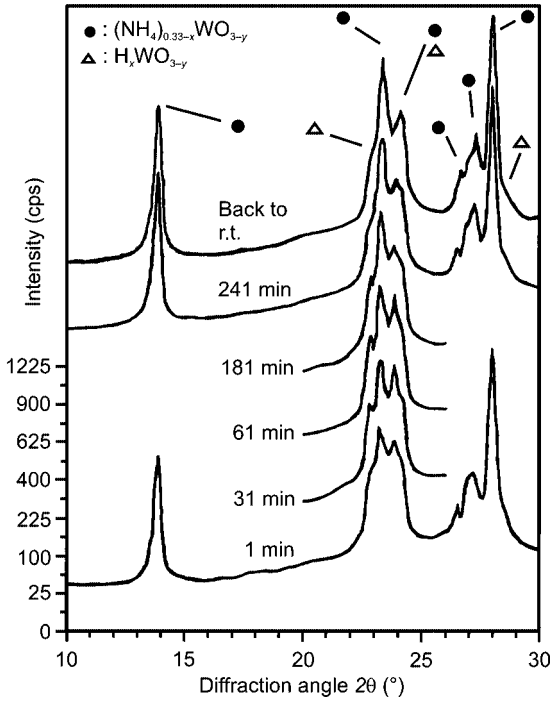

Figure 1. In situ HT-XRD patterns at 400 °C after rapid heating (100 °C min^{-1}) of APT in 10% H_2/He.

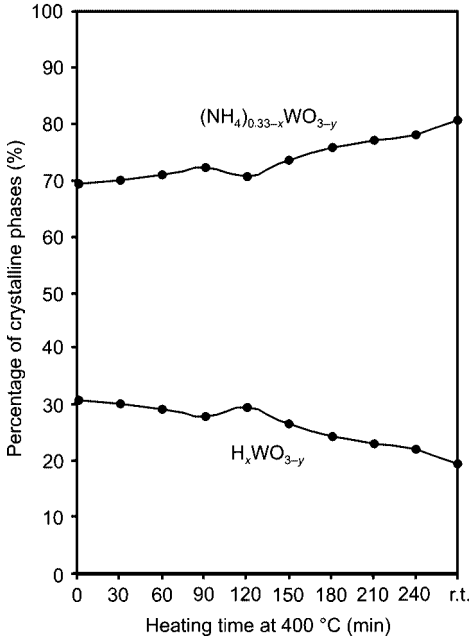

Figure 2. Amount of the formed crystalline tungsten bronzes from APT at 400 °C after rapid heating (100 °C min^{-1}) in 10% H_2/He.

During consecutive heating at 400 °C, the sample became more crystalline. This is indicated by the growth in intensity of reflections from both the hexagonal and tetragonal bronzes (Figure 1). On the other hand, the ratio of the hexagonal phase increased steadily (Figure 2). A further increase in the crystallinity of the sample and the amount of the hexagonal bronze (80%) accompanied cooling of the sample to room temperature (r.t.), which followed the 4 h isothermal heating period.

Our present study, as well as a comparison of earlier results,[1,2,7,37–46] shows that the heating conditions of APT in a reducing gas influence the formation of the bronzes, i.e. formation of the hexagonal bronze is favoured when APT is heated rapidly whereas for the formation of the tetragonal bronze, slow heating is favourable. We propose an explanation in terms of structure for this phenomenon.

The structure of APT is basically determined by the paratungstate ion, $[H_2W_{12}O_{42}]^{10-}$, which is built up from twelve WO_6 octahedra. These large ions are bound together by water molecules and ammonium ions.[48] When annealing APT at 250–300 °C (in fact this is the third main decomposition step of APT[1,2,37]), ammonia and water are released, structural collapse and rearrangement take place, i.e. some WO_6 octahedra from separate paratungstate ions become linked together and an amorphous phase is formed.[49] In this structure, a certain number of water molecules, ammonium ions as well as ammonia molecules are trapped and therefore cannot be released in this temperature region. From the amorphous phase, tungsten bronzes and then tungsten oxides form on further heating at 300–600 °C.

We suppose that the heating rate of APT determines the process of WO_6 octahedra linking and the amount of trapped molecules and ions. This then also determines the possibility of the formation of hexagonal and tetragonal

bronzes. Ammonia molecules and ammonium ions fit in the hexagonal channels of HATB the best. Therefore, the faster APT is heated, the more ammonia molecules and ammonium ions (as well as water molecules) are trapped in the cages between the WO_6 octahedra. This results in a higher proportion of hexagonal bronze.

The growth in the amount of HATB during the isothermal period must also be explained. One solution might be that the tetragonal bronze becomes transformed into the hexagonal material.[39] The other possibility is that right after (1 min; Figure 2) the rapid heating of APT, only a part of the sample crystallised. Since under such circumstances the formation of the hexagonal phase seems to be favoured, during the isothermal period, when the other part of the sample also crystallised, HATB was formed to a greater extent than THTB resulting in a growth in the percentage of the hexagonal bronze.

It should be mentioned that we observed only a phase mixture at all stages of the reaction and that the hexagonal bronze was accompanied by small amounts of the tetragonal bronze even after 4 h of annealing. We assume that the difference of the decomposition conditions for APT in a furnace and in a high-temperature camera may be the reason why a monophasic HATB finally did not form in our experiments.

However, we clearly detected that during fast heating and then during isothermal heating of APT, much more hexagonal bronze than tetragonal bronze formed. We also observed that during the isothermal stage the sample became more crystalline. Our results and assumptions together with earlier studies[41–46] thus show that when HATB is required in a highly crystalline, monophasic form, APT has to be heated rapidly, preferably at 400 °C in a reducing gas, and kept under these conditions for several hours, which in practice corresponds to heating APT in a furnace.

It is very interesting that in air formation of the tetragonal hydrogen tungsten bronze was not observed as described earlier and that hexagonal ammonium tungsten bronze was accompanied by an X-ray amorphous phase and/or by crystalline monoclinic, orthorhombic or hexagonal WO_3.[1,2,33–37] In this case, oxidation might also have an effect on the linking process of paratungstate ions, which should be responsible for the absence of the tetragonal bronze during the decomposition sequence of APT in air.

Characterisation of Hexagonal Ammonium Tungsten Bronze

In order to check our model of how highly crystalline, monophasic hexagonal ammonium tungsten bronze is formed through the partial reduction of APT, ammonium paratungstate tetrahydrate was annealed at 400 °C for 6 h in H_2. The structure and composition of the resultant HATB sample were determined by high-precision powder XRD, XPS, chemical analysis and ^{1}H-MAS-NMR spectroscopy.

Characterisation of Hexagonal Ammonium Tungsten Bronze by High-Precision XRD

XRD analysis showed that the HATB sample contained only the hexagonal ammonium tungsten bronze phase, which was identified by the ICDD 42-0452 card in space group $P6_3/mcm$, no. 193.[46] The sample was highly crystalline [the signal/background ratio for the (2,0,0) reflection was 6050 cps/60 cps] and an X-ray amorphous phase was not detected. Thus, a monophasic, highly crystalline hexagonal ammonium tungsten bronze could be successfully produced by partial thermal reduction of APT, in agreement with our model.

To check the cell parameter refining program, we recalculated the cell parameters of the title compound on the basis of the measured reflections of HATB found in the literature[8,44,46] and this showed the reliability of our program (Table 1). The slight difference in literature cell parameters[8,44,46] might have been caused mostly by the differences in the compositions of hexagonal ammonium tungsten bronze samples.[5]

In order to obtain precise XRD data, we used all the simulated reflections of the $P6_3/mcm$, no. 193 space group for finding and indexing the reflections in the measured XRD pattern of the HATB sample. The simulated reflections were calculated with PulverX using cell parameters of HATB reported by Dickens et al.[44] Deconvolution of peaks, base line correction, splitting of peaks from Cu-$K_{\alpha1}$ and -$K_{\alpha2}$ radiation, profile fitting and, finally, correction of reflections on the basis of an Si internal standard were then performed. The obtained reflections of HATB are listed in Table 2.

The following cell parameters of the HATB sample were obtained: $a = 0.7381 \pm 0.0001$ nm, $c = 0.7540 \pm 0.0002$ nm.

While we could detect all the measurable 77 reflections of HATB, Kiss et al.[8] observed 49 reflections, Dickens et al.[44] listed 20 and Volkov[46] detected 25 of them. Interestingly, Kiss et al.[8] reported indices (3,0,1) and (5,0,3), which are in contrast to the extinction rule of the space group $P6_3/mcm$, no. 193.

Characterisation of Hexagonal Ammonium Tungsten Bronze by XPS

In tungsten bronzes, the tungsten atoms may appear in different oxidation states.[1,2] To check this for our HATB

Table 1. Recalculation of cell parameters of HATB samples for which *d* values have been previously published.[8,44,46]

Source	Compound	a [nm]	σ_a [nm]	c [nm]	σ_c [nm]
Ref.[46] ICDD 42-0452	$(NH_4)_{0.33}WO_3$	0.7392	0.0002	0.7512	0.0003
Recalculated ref.[46]		0.7391	0.0001	0.7512	0.0002
Ref.[44]	$(NH_4)_{0.25}WO_3$	0.7388	0.0003	0.7551	0.0006
Recalculated ref.[44]		0.7388	0.0003	0.7550	0.0006
Ref.[8]	$(NH_4)_{0.1135}WO_{2.9832}\cdot(H_2O)_{0.14}$	0.7389	not given	0.7514	not given
Recalculated ref.[8]		0.7379	0.0005	0.7508	0.0009

Table 2. Powder XRD data of HATB.

d [nm]	I/I_0 [%]	*hkl*	*d* [nm]	I/I_0 [%]	*hkl*
0.6407	41.4	100	0.1277	0.3	500
0.3771	66.7	002	0.1267	0.4	323
0.3696	17.9	110	0.1257	0.8	006
0.3308	7.5	111	0.1233	0.9	106
0.3246	18.8	102	0.1226	0.9	330
0.3197	100.0	200	0.1220	3.0	413
0.2638	9.7	112	0.1219	3.0	404
0.2439	55.9	202	0.1216	1.5	331
0.2413	2.5	210	0.1210	2.1	502
0.2303	4.4	211	0.1209	1.7	420
0.2132	2.8	300	0.1188	0.5	116
0.2076	1.5	113	0.1170	1.8	206
0.2035	2.6	212	0.1168	1.5	332
0.1885	8.7	004	0.1158	0.9	324
0.1857	2.9	302	0.1152	2.8	422
0.1846	17.0	220	0.1149	2.0	315
0.1808	2.9	104	0.1148	1.5	510
0.1774	4.6	310	0.1136	2.2	511
0.1741	2.0	213	0.1121	0.6	414
0.1726	6.3	311	0.1114	0.2	216
0.1678	2.8	114	0.1105	1.1	333
0.1657	15.6	222	0.1098	0.9	512
0.1624	18.1	204	0.1082	0.2	306
0.1603	6.5	312	0.1066	0.6	600
0.1599	5.1	400	0.1052	0.3	325
0.1484	1.7	214	0.1050	0.2	430
0.1473	6.9	402	0.1045	2.0	513
0.1470	3.1	320	0.1040	0.9	431
0.1450	3.3	313	0.1038	1.5	226
0.1441	0.6	321	0.1035	0.5	117
0.1413	0.9	304	0.1030	0.6	334
0.1400	0.7	115	0.1026	0.6	316
0.1395	0.8	410	0.1025	1.0	602
0.1374	2.5	411	0.1024	0.4	415
0.1367	0.6	322	0.1023	0.4	520
0.1320	7.2	224	0.1018	2.7	424
0.1310	1.1	412	0.1015	0.7	521
0.1292	1.8	314	0.1011	0.1	432
0.1280	0.1	215			

sample, the WO_3 reference sample was investigated first. Besides O atoms (O1s = 530.7 eV) only W^{VI} atoms were detected (Figure 3a), the W4f values of which ($W4f_{7/2}$ = 36.9 eV and $W4f_{5/2}$ = 34.8 eV) were in agreement with earlier results.[27,50,51]

After refining the XPS spectrum belonging to the HATB sample (Figure 3b), W^{IV} atoms ($W4f_{7/2}$ = 35.2 eV and $W4f_{5/2}$ = 33.2 eV) and W^{V} atoms ($W4f_{7/2}$ = 35.9 eV and $W4f_{5/2}$ = 33.5 eV) were also observed besides W^{VI} atoms.[52–54] Zhan et al.[32] also investigated a hexagonal ammonium tungsten bronze sample by XPS but they did not report the presence of W^{IV} and W^{V} atoms.

Furthermore, in our HATB sample, NH_3 molecules (N1s = 399.7 eV) were also detected in addition to NH_4^+ ions (N1s = 401.9 eV).[50,51] Up to this time ammonia molecules were only detected in HATB by ^{1}H-MAS-NMR spectroscopy[4,5] whereas they were not detected by XPS.[32]

Depth profiling by Ar^+ ion sputtering was not informative because sputtering distorted the structure so much that, due to oxygen loss, even W^0 species ($W4f_{7/2}$ = 32.5 eV and $W4f_{5/2}$ = 30.5 eV) appeared.[54–56]

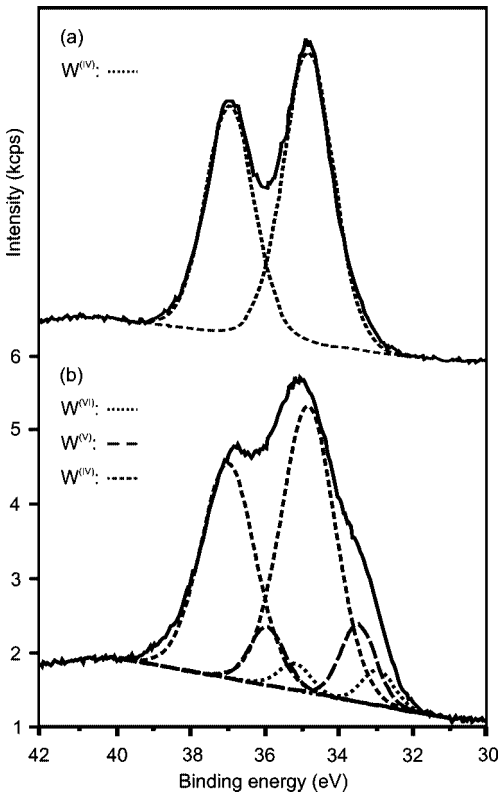

Figure 3. XPS spectra of (a) WO_3 and (b) HATB.

Chemical Analysis of Hexagonal Ammonium Tungsten Bronze

In order to determine the composition of the HATB sample, it was first heated at 800 °C in argon in a Setaram TG-DTA 92 thermobalance to form WO_{3-x} and was then heated at 800 °C in air to form WO_3. From the corresponding weight changes, the W and O contents of the sample were calculated. The N content was determined by titration of the ammonia released when the HATB sample was heated in nitrogen. The ratio of NH_4^+ ions to NH_3 molecules was measured by XPS. The total amount of H_2O present in the sample was calculated by complementing to 100% (m/m). The weight loss of the sample up to 100 °C, i.e. corresponding to adsorbed water was not taken into account when calculating the stoichiometry. Thus, the formula of the HATB sample was determined as $(NH_4)_{0.07}(NH_3)_{0.04}(H_2O)_{0.09}WO_{2.95}$. XPS analysis showed no impurities in the sample.

In the case of HATB samples, for which cell parameters and *d* values were published previously[8,44,46] (Table 1), the chemical analysis of samples was not detailed enough. The presence of NH_3 molecules was not checked in any of the reports corresponding to refs.[8,44,46] and the rate of reduction, i.e. the oxygen index, was not taken into account in refs.[44,46].

Characterisation of Hexagonal Ammonium Tungsten Bronze by ^{1}H-MAS-NMR Spectroscopy

Because of the possible presence of some proton-containing species (NH_3, NH_4^+, H_2O and OH group) in hexagonal

ammonium tungsten bronze, the HATB sample was also characterised by solid-state ^{1}H NMR spectroscopy.

In the ^{1}H-MAS-NMR spectrum of the WO_3 reference sample, only a small peak was observed at δ = 0.8 ppm, which was also noticeable in the ^{1}H-MAS-NMR spectrum of HATB (Figure 4). Since this peak was also present in the ^{1}H-MAS-NMR spectrum of the sample holder, we could not check the presence of OH groups on the surface of WO_3 and HATB particles.[4,5,57]

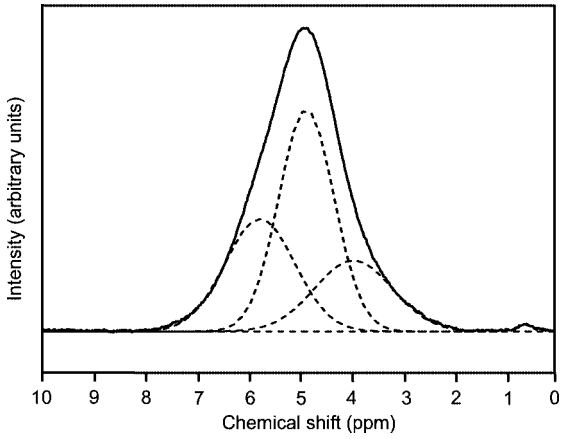

Figure 4. ^{1}H-MAS-NMR spectrum of HATB.

In the^{1}H-MAS-NMR spectrum of HATB, the large peak at $\delta \approx 5$ ppm seemed to be asymmetric and we could not fit it properly with one or two but only with three peaks. The peak at δ = 4.9 ppm was assigned to the ammonium ions situated in the hexagonal channels, in accordance with ref.[5] We suppose that the peak at δ = 5.8 ppm is due to ammonia molecules in the hexagonal channels, an idea which is also supported by our XPS measurements and also by earlier results.[5] The peak at δ = 4.0 ppm may come from water molecules bound to the surface of or inside the bronze particles.

Conclusions

On the basis of in situ HT-XRD measurements and earlier results,[1,2,7,37–45] we propose that the heating program of APT influences the process of linking of WO_6 octahedra of paratungstate ions. This probably determines the likelihood, as a result of structural factors, of the formation of hexagonal ammonium tungsten bronze. Formation of monophasic hexagonal bronze is favoured the most when APT is heated rapidly at 400 °C in a reducing gas. On the basis of this model, the preparation of a highly crystalline, monophasic HATB sample was successful.

Chemical analysis of the resultant hexagonal ammonium tungsten bronze sample showed a composition of $(NH_4)_{0.07}(NH_3)_{0.04}(H_2O)_{0.09}WO_{2.95}$. The presence of W^{IV}, W^{V} and W^{VI} species detected by XPS supports the electron-conducting properties while the presence of NH_3 molecules and NH_4^+ ions detected by XPS and ^{1}H-MAS-NMR spectroscopy supports the proton-conducting properties of the title compound. With powder XRD analysis more reflections of hexagonal ammonium tungsten bronze were detected than previously observed.

Experimental Section

Ammonium Paratungstate Tetrahydrate: Ammonium paratungstate tetrahydrate (H. C. Starck GmbH), $(NH_4)_{10}[H_2W_{12}O_{42}]\cdot 4H_2O$ (ICDD 40-1470) was used as purchased (analysis: measured WO_3 89.6%, NH_3 5.1%; calculated WO_3 88.8%, NH_3 5.4%). XRD measurements did not show any impurities in the APT sample.

Hexagonal Ammonium Tungsten Bronze: Hexagonal ammonium tungsten bronze was produced by annealing APT at 400 °C for 6 h in H_2 since, on the basis of earlier results[43–45] and our HT-XRD measurements, these conditions seemed to be the best for the formation of highly crystalline, monophasic HATB.

Tungsten Trioxide: Monoclinic tungsten trioxide, WO_3 (ICDD 83-0951), was produced as a reference sample for XPS and ^{1}H-MAS-NMR spectroscopic analysis by heating APT at 600 °C for 2 h in air. XRD, XPS and ^{1}H-MAS-NMR spectroscopic measurements did not show any impurities in the WO_3 sample.

In situ High-Temperature Powder X-ray Diffraction (HT-XRD): HT-XRD patterns were recorded with a device consisting of a Müller Mikro 111 generator, a Philips PW 1710 diffractometer control unit and a Philips PW 1050 goniometer between 2θ = 10–30° and 20–26° at (0.02° per 0.5 s) with Cu-$K_{\alpha 1,2}$ radiation. Heating of samples was performed in an Anton Paar HTK 16 high-temperature camera in flowing 10% H_2/He. Deconvolution of peaks, base-line correction, splitting of peaks from Cu-$K_{\alpha 1}$ and -$K_{\alpha 2}$ radiation as well as profile fitting were carried out using Profit for Windows 1.0. The relative ratio of the crystalline phases was calculated by semiquantitative phase analysis.

Powder X-ray Diffraction (XRD): X-ray diffraction pattern of the title compound was recorded with a Philips MPD 1880 X-ray diffractometer using Si (ICDD 27-1402) as an internal standard between 2θ = 5 and 100° at (0.01° per 3 s) with Cu-$K_{\alpha 1,2}$ radiation. The same program and method were used to obtain the Cu-$K_{\alpha 1}$ reflections as in the case of in situ HT-XRD experiments. Measured reflections were indexed on the basis of simulated reflections of the $P6_3/mcm$, no. 193 space group, which were calculated by PulverX using cell parameters of HATB reported by Dickens et al.[44] A linear interpolation was made between the deviations of measured and standard d values at each Cu-$K_{\alpha 1}$ reflection belonging to the Si internal standard and, using the function obtained this way, the d values of HATB sample were corrected. The cell parameters of hexagonal ammonium tungsten bronze were refined using a gwbasic language program, which used non-linear fitting (least square of $1/d^2$, Gauss–Newton–Marquardt method) without weighting.[58]

X-ray Photoelectron Spectroscopy (XPS): XPS data were collected with a VG Microtech instrument consisting of an XR3E2 X-ray source, a twin anode (Mg-K_α and Al-K_α) and a CLAM 2 hemispherical analyser using Mg-K_α radiation. Survey scans were obtained in the 0–1100 eV range with a 20 eV pass energy at 0.4 eV per 0.1 s. Detailed scans were recorded with a 50 eV pass energy at 0.05 eV per 1.5 s. The spectrometer was calibrated by using the binding energy of the C 1s line (284.5 eV).

Solid-State ^{1}H NMR Spectroscopy (^{1}H-MAS-NMR): ^{1}H-MAS-NMR spectra were recorded with a Varian Unity 300 spectrometer supplied with a Doty XC5 solid-phase ^{1}H head at a rotor spinning frequency of 4000 Hz in an XC5 insert (special sample holder), which was set inside an Si_3N_4 rotor.

Acknowledgments

G. Szalontai (NMR Laboratory, Pannon University, Veszprém, Hungary) as well as V. K. Josepovits and H. Lovas (Department of Atomic Physics, Budapest University of Technology and Economics, Hungary) are greatly acknowledged for their help in performing ^{1}H-MAS-NMR and XPS measurements, respectively. One of the authors (I. M. S.) is grateful for an Aschner scholarship of GE Hungary ZRt, GE Consumer & Industrial Lighting.

[1] E. Lassner, W.-D. Schubert, *Tungsten. Properties, Chemistry, Technology of the Element, Alloys, and Chemical Compounds*, Kluwer Academic/Plenum Publishers, New York, **1999**.
[2] "Special Issue on the Chemistry of Non-Sag Tungsten" (Eds.: L. Bartha, E. Lassner, W.-D. Schubert, B. Lux), *Int. J. Refract. Met. Hard Mater.* **1995**, *13*, 1–164.
[3] E. Pink, L. Bartha, *The Metallurgy of Doped/Non-Sag Tungsten*, Elsevier, London, **1989**.
[4] H.-J. Lunk, B. Ziemer, M. Salmen, D. Heidemann, *Int. J. Refract. Met. Hard Mater.* **1993–1994**, *12*, 17–26.
[5] H.-J. Lunk, M. Salmen, D. Heidemann, *Int. J. Refract. Met. Hard Mater.* **1998**, *16*, 23–30.
[6] A. Lackner, T. Molinari, P. Paschen, *Scand. J. Metall.* **1996**, *25*, 115–121.
[7] J. W. van Put, T. W. Zegers, *Int. J. Refract. Met. Hard Mater.* **1991**, *10*, 115–122.
[8] B. A. Kiss, G. Rom Berendné, G. Gyarmathy, Z. Kutasi Feketéné, *Magy. Kem. Foly* **1987**, *93*, 97–106.
[9] L. Bartha, G. Gyarmati, B. A. Kiss, T. Németh, A. Salamon, T. Szalay, *Acta Chim. Acad. Sci. Hung.* **1979**, *101*, 127–138.
[10] C. G. Grandqvist, *Handbook of Inorganic Electrochromic Materials*, Elsevier, Amsterdam, **1995**.
[11] C. G. Granqvist, *J. Eur. Ceram. Soc.* **2005**, *25*, 2907–2912.
[12] A. Azens, E. Avendano, J. Backholm, L. Berggren, G. Gustavsson, R. Karmhag, G. A. Niklasson, A. Roos, C. G. Granqvist, *Mater. Sci. Eng., B* **2005**, *119*, 214–223.
[13] A. A. Argun, P. H. Aubert, B. C. Thompson, I. Schwedeman, C. L. Gaupp, J. Hwang, N. J. Pinto, D. B. Tanner, A. G. MacDiarmid, J. R. Reynolds, *Chem. Mater.* **2004**, *16*, 4401–4412.
[14] C. G. Granqvist, A. Avendano, A. Azens, *Thin Solid Films* **2003**, *442*, 201–211.
[15] G. V. Kunte, U. Ail, S. A. Shivashankar, A. M. Umarji, *Bull. Mater. Sci.* **2005**, *28*, 243–248.
[16] I. Tsuyomoto, T. Kudo, *Sens. Actuators, B* **1996**, *30*, 95–99.
[17] G. Shaw, I. P. Parkin, K. F. E. Pratt, D. E. Williams, *J. Mater. Chem.* **2005**, *15*, 149–154.
[18] C. J. Jin, T. Yamazaki, Y. Shirai, T. Yoshiwaza, T. Kikuta, N. Nakatani, H. Takeda, *Thin Solid Films* **2005**, *474*, 255–260.
[19] R. Ionescu, A. Hoel, C. G. Granqvist, E. Llobet, P. Heszler, *Sens. Actuators, B* **2005**, *104*, 124–131.
[20] X. L. Li, T. J. Lou, X. M. Sun, Y. D. Li, *Inorg. Chem.* **2004**, *43*, 5442–5449.
[21] L. Zhuang, X. Xu, H. Shen, *Surf. Coat. Technol.* **2003**, *167*, 217–220.
[22] W. Han, M. Hibino, T. Kudo, *Solid State Ionics* **2000**, *128*, 25–32.
[23] M. S. Wittingham, *Solid State Ionics* **2004**, *168*, 255–263.
[24] B. Gérand, L. Seguin, *Solid State Ionics* **1996**, *84*, 199–204.
[25] L. Huao, H. Zhao, F. Mauvy, S. Fourcade, C. Labrugere, M. Pouchard, J.-C. Grenier, *Solid State Sci.* **2004**, *6*, 679–688.
[26] B. Schlasche, R. Schollhorn, *Rev. Chim. Miner.* **1982**, *19*, 534–544.
[27] O. Y. Khyzhun, Y. M. Solonin, V. F. Dobrovolsky, *J. Alloys Compd.* **2001**, *320*, 1–6.
[28] J. Pfeifer, C. Balázsi, B. A. Kiss, B. Pécz, A. L. Tóth, *J. Mater. Sci. Lett.* **1999**, *18*, 1103–1105.
[29] W. Han, M. Hibino, T. Kudo, *Bull. Chem. Soc. Jpn.* **1998**, *71*, 933–937.
[30] T. E. Gier, D. C. Pease, A. W. Sleight, T. A. Bither, *Inorg. Chem.* **1968**, *7*, 1646–1647.
[31] A. Michailovski, F. Krumeich, G. R. Patzke, *Chem. Mater.* **2004**, *16*, 1433–1440.
[32] J. H. Zhan, X. G. Yang, Y. Xie, B. F. Li, Y. T. Qain, Y. B. Jia, *Solid State Ionics* **1999**, *126*, 373–377.
[33] J. Madarász, I. M. Szilágyi, F. Hange, G. Pokol, *J. Anal. Appl. Pyrolysis* **2004**, *72*, 197–201.
[34] N. E. Fouad, A. K. H. Nohman, M. A. Mohamed, M. I. Zaki, *J. Anal. Appl. Pyrolysis* **2000**, *56*, 23–31.
[35] Z. Zhang, M. Muhammed, *Thermochim. Acta* **2003**, *400*, 235–245.
[36] A. B. Kiss, L. Chudik-Major, *Acta Chim. Acad. Sci. Hung.* **1973**, *78*, 237–251.
[37] O. Kirilenko, F. Girgsdies, R. E. Jentoft, T. Ressler, *Eur. J. Inorg. Chem.* **2005**, *11*, 2124–2133.
[38] I. M. Szilágyi, J. Madarász, F. Hange, G. Pokol, *Solid State Ionics* **2004**, *172*, 583–586.
[39] M. Mészáros, J. Neugebauer, F. Hange, *High Temp. Mater. Processes* **1996**, *15*, 111–115.
[40] N. E. Fouad, A. K. H. Nohman, M. I. Zaki, *Thermochim. Acta* **2000**, *343*, 139–143.
[41] R. C. T. Slade, P. G. Dickens, D. A. Claridge, D. J. Murphy, T. K. Halstead, *Solid State Ionics* **1990**, *38*, 201–206.
[42] L. D. Clark, M. S. Wittingham, R. A. Huggins, *J. Solid State Chem.* **1972**, *5*, 487–493.
[43] J. Bludská, J. Vondrák, I. Jakubec, *Electrochim. Acta* **1994**, *39*, 2045–2048.
[44] P. G. Dickens, A. C. Halliwell, D. J. Murphy, M. S. Wittingham, *Trans. Faraday Soc.* **1971**, *67*, 794–800.
[45] Y. Yamamoto, S. Yamada, S. Honkawa, N. Shigaki, *Funtai oyobi Funmatsu Yakin* **1993**, *40*, 1126–1130.
[46] a) V. L. Volkov, *Izv. Akad. Nauk SSSR. Neorg. Mater. (Russ.)* **1990**, *26*, 125–129; b) V. L. Volkov, *Inorg. Mater. (Engl. Transl.)* **1990**, *26*, 101; c) $(NH_4)_{0.33}WO_3$, International Centre for Diffraction Data (ICDD), file no. 42-0452.
[47] I. M. Szilágyi, J. Madarász, F. Hange, G. Pokol, to be published.
[48] H. D'Amour, R. Allman, *Z. Kristallogr.* **1972**, *136*, 23–47.
[49] M. A. Mohamed, S. A. A. Mansour, M. I. Zaki, *Thermochim. Acta* **1989**, *138*, 309–317.
[50] *Handbook of X-ray Photoelectron Spectroscopy* (Eds.: C. D. Wagner, W. M. Riggs, L. E. Davis, J. F. Moulder, G. E. Muilenberg), Perkin–Elmer Corporation, Division of Electronics Division, Minessota, **1979**.
[51] B. V. Crist, *Handbook of Monochromatic XPS Spectra*, vol. 1 ("The Elements and Nature Oxides"), XPS International, California, **1999**.
[52] A. Henningson, H. Rensmo, A. Sandell, S. Södergen, H. Siegbahn, *Thin Solid Films* **2004**, *461*, 237–242.
[53] D. Gogova, K. Gesheva, A. Kakanakova-Georgieva, M. Surtchev, *Eur. Phys. J. Appl. Phys.* **2000**, *11*, 167–174.
[54] H. Y. Wong, C. W. Ong, R. W. M. Kwok, K. W. Wong, S. P. Wong, W. Y. Cheung, *Thin Solid Films* **2000**, *376*, 131–139.
[55] W. B. Cross, I. P. Parkin, S. A. O'Neil, P. A. Williams, M. F. Mahon, K. C. Molloy, *Chem. Mater.* **2003**, *15*, 2786–2796.
[56] S. Santucci, C. Cantalini, M. Crivellari, L. Lozzi, L. Ottaviano, M. Passacantando, *J. Vac. Sci. Technol. A* **2000**, *18*, 1077–1082.
[57] J. Z. Hu, J. H. Kwak, J. E. Herrera, Y. Wang, C. H. F. Peden, *Solid State Nucl. Magn. Reson.* **2005**, *27*, 200–205.
[58] P. Valkó, S. Vajda, *Advanced Scientific Computing in BASIC with Applications in Chemistry, Biology and Pharmacology*, Elsevier Science Publishers, New York, **1989**.

Received: September 29, 2005
Published Online: July 24, 2006

